ADVANCES IN ATMOSPHERIC SCIENCES, VOL. 23, NO. 5, 2006, 678–692

On the Climatology of Persistent Heavy Rainfall Events in China

TANG Yanbing* (汤燕冰), GAN Jingjing (甘晶晶), ZHAO Lu (赵 璐), and GAO Kun (高 坤)

Department of Earth Sciences, Zhejiang University, Hangzhou 310027

(Received 25 August 2005; revised 25 May 2006)

ABSTRACT

Persistent heavy rainfall events (PHR events) comprise one category of weather- and climate- related extreme events. Based on daily rainfall data measured in China during the period of 1951–2004, several quantitative criteria were developed to define PHR events by means of their precipitation intensity, temporal duration, spatial extent and persistence. Then a semi-objective classification based on these criteria was applied to summer daily rainfall data to identify all PHR events. A total of 197 events were observed during the study period. All events were further classified into 5 categories according to their comprehensive intensity; into 3 types according to their circulation regime; and into 8 groups according to the geographic locations of their rainbands. Based on these different classifications, finally, the behaviors of 130 PHR events identified as the most severe, severe and moderate categories since the year of 1951, including characteristics of the spatial and temporal distributions of their frequencies, intensities, and rainbands, were investigated in order to present a comprehensive description of the PHR events. The results will be helpful to the future study of revealing and understanding the processes that govern the production of the PHR events and to the improvement of the forecasts of the PHR events.

Key words: Persistent heavy rainfall, extreme precipitation event, China, climatology

doi: 10.1007/s00376-006-0678-x

1. Introduction

Persistent heavy rainfall events (PHR events hereafter) indicate one type of extreme in weather and climate that unquestionably have large impacts on China's economy and society. PHR events are distinguishable from other types of extreme precipitation by several observable attributes: high intensity, broad extent, and persistent and stable existence. PHR events are responsible for most prolonged and extensive floodings in China, especially accounting for many catastrophic floods, such as that which occurred in 1998 in the Yangtze River Basin (Zhang et al. 2002). PHR prediction continually challenges current research efforts.

As significant causes of weather-related disasters, PHR events have received much attention. Considerable research has been devoted to their causes, behaviors, and variations. However, much of this research, including diagnostic analysis and dynamic simulations, has focused on a particular case that occurred in some specific periods (e.g., Mei-yu season) and on comparatively restricted geographical areas (e.g., the middle and lower reaches of the Yangtze River valley). Studies of PHR events occurring in the years 1991 (Zhang et al., 2002), 1998 (Zhang et al., 2002; Xiong et al., 2003; Liu et al., 2002) and 1999 (Zhang et al., 2002; Guo et al., 2004) provide examples. So far, no one has comprehensively investigated the behaviors of the persistent heavy rainfall events throughout China under the global climate change (Karl and Trenberth, 2003, Trenberth and et al., 2003) with the help of the daily rainfall observations over a longer period (more than 50 years). How are the PHR events spatially and temporally distributed during the study period? What are the favorable environmental conditions for such extreme precipitation events? How do their frequency and intensity change under the global climate change? So far, answers for these questions are still unclear.

In this study, we will examine all PHR events that have occurred within China since 1951. Our purpose is to characterize these events, place them into a regional framework, and determine how selected attributes and behaviors differ between regions.

Section 2 describes the data used in this study. Section 3 deals with definitions of PHR events and related methodological approaches. Section 4 presents the study results, whereas section 5 offers a summary

*E-mail: y_tang@css.zju.edu.cn

of this study.

2. Data

The primary rainfall data utilized in this study consist of summer (April–August) daily totals from 743 weather stations operating in China during the period 1951–2004 (Fig. 1). The lengths of available records differ from station to station. From 1951 to 1952, only 139 recorded stations (shown as circles in Fig. 1) existed. From 1953 to 1956, 330 stations (shown as triangles in Fig. 1) were available. After 1957, more than 600 stations (shown as dots in Fig. 1) were available. For this study, both individual station records and derived gridded data were employed. The gridded dataset of daily rainfall was constructed by objectively interpolating all available records for a given day into 30 km by 30 km grid boxes within the scope of Fig. 1. The long-term mean used in this study was based on the 30-yr period 1971–2000. Large-scale circulation data during the same period were provided by the National Centers for Environmental Prediction-National Center for Atmospheric Research (NCEP-NCAR) reanalysis (Kalnay et al., 1996).

3. Definitions and methods

The first requirement was to define what a persistent heavy rainfall event was since no commonly agreed upon definition exists in the literature. In order to identify PHR events based on gridded daily rainfall data, several criteria were developed to quantify rainfall intensity, duration and extent. Then PHR events were identified by means of these quantitative criteria.

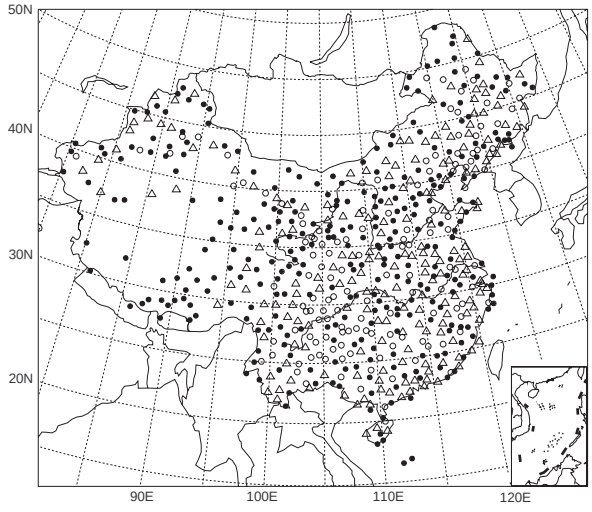

Fig. 1. Locations of the observation stations. The open circles indicate where the daily precipitation observations begin between the year of 1951–1952; the triangles between 1953–1956; and the dots since 1957.

Table 1. Daily rainfall intensity categories.

Category	1951–1952	1953–1956	1957–2004
Heavy Rain Day (D25)	9	18	36
Heavier Rain Day (D50)	6	12	24
Extremely Heavy Rain Day (D100)	3	6	12

As mentioned above, PHR events are known for their high intensity, duration, stability, and extent. The criteria developed to signify the intensity, duration and extent of PHR events from different aspects included:

(1) Intensity criteria

Similar to the categorization of station daily precipitation intensity set by the China Meteorological Administration (CMA)*, we defined three categories to quantify area daily rainfall intensity based on the gridded daily rainfall fields. Considering the varied availability of daily rainfall records for different periods (Table 1), slightly different standards were used. A heavy rain day (D25) was defined as a day with total precipitation between 25–50 mm over at least 9 contiguous grid cells for the period 1951–1952; at least 18 contiguous cells for the period 1953–1956 and at least 36 contiguous cells for the remaining period. A heavier rain day (D50) was defined as a day with total precipitation between 50–100 mm over at least 6 contiguous grid cells for the period of 1951–1952; at least 12 contiguous cells for 1953–1956 and 24 contiguous cells for the rest. An extremely heavy rain day (D100) was defined as a day with total precipitation exceeding 100 mm over at least 3 contiguous grid cells for the period of 1951–1952; at least 6 contiguous cells for 1953–1956 and 12 contiguous cells for the remaining period.

(2) Extent Criterion

We used the size of the event rainband as a surrogate for the extent of an event. The event rainband in this study was defined as the area of contiguous grid cells that received more than 100 mm precipitation over the duration of an event.

(3) Duration Criteria

The duration of a PHR event expresses the length of time over which the event occurs. For this study,

*The China Meteorological Administration categorizes daily precipitation (P) into five intensity groups. They are, $P < 10$ mm d^{-1} (light rain), 10 mm d^{-1} $\leqslant P <$ 25 mm d^{-1} (moderate rain), 25 mm d^{-1} $\leqslant P <$ 50 mm d^{-1} (heavy rain), 50 mm d^{-1} $\leqslant P <$ 100 mm d^{-1} (heavier rain) and $P \geqslant$ 100 mm d^{-1} (extremely heavy rain).

time length was expressed in number of days. By definition, the duration of a PHR event was subject to the following qualifications:

(a) An event must last more than 4 days, starting with a D100 or a D50;

(b) An event must consist of more than three D100s and four D50s during the period;

(c) The percentage of the D25s must constitute less than 20% of the duration of an event, and no day below D25 is allowed;

(d) The maximum accumulated rainfall for an event must exceed 250 mm.

Relying on these criteria, we identified more than 200 PHR events in the daily precipitation records. Following verification, however, the total number of events was subsequently reduced to 197. Verification was performed chiefly on daily rainfall fields. The factors considered included shifting of the daily rainband, the daily variation of an event's circulation and the consistency between events identified simultaneously in different regions. As noted, PHR events are known for their long durations and persistent precipitation. Thus, the position of a daily rainband for a specific case should be relatively stable. If the daily position of an event's rainband shifted more than 2 degrees in any direction, the case was deleted.

To facilitate further study of PHR events, both gridded and station daily rainfall data were used to define a comprehensive intensity index after defining the events. To do this, three indexes, the ratio of total rainfall over a grid to mean summer rainfall total over the same grid (A hereafter), the ratio of the number of heavy rain days for a station to mean summer heavy rain days for the same station (B hereafter) and the percentage of stations located in an event's rainband with over 300 mm total rainfall (C hereafter), had to be developed (Table 2). Indexes A and B were designed to measure the magnitude of the relative event intensity to the climate. Moreover, both can be used to compare events occurring in different regions since they are dimensionless. They eliminate geographical differences in mean annual summer precipitation and numbers of D50. It should be indicated that, considering the important contribution of the extent of an event rainband to the severity of a PHR event, the sum, instead of the average, of all grid cells or stations within an event rainband was used to define A and B. High values of A or B indicate high contributions of total rainfall or D50 in the corresponding climate. Index C describes the stability of an event rainband. A high value of C means that the event rainband with heavier precipitation is relatively less dispersed. After their definition, events for each index were ranked from 1 to 197. Number 1 corresponds to the most severe condition and number 197 the least severe. Based on these three rankings, the following comprehensive intensity index was built (explained in Table 2):

$$\text{Comprehensive Intensity Index} = \text{Rank A} + \text{Rank B} + \text{Rank C} \quad (1)$$

Based on a rule of thumb for any normal distribution (Trialo, 2003), we grouped PHR events into five categories (Table 3) according to their values of the comprehensive intensity index defined as Eq. (1), since the intensity indexes of 197 PHR events are roughly distributed normally. The averaged major attributes of the five categories of PHR events are listed in Table. 4. The attributes include the length in days that directly describes the persistence of the events; the area-weighted sum of the total rainfall over the event rainband, indexes A and B that directly reflect the severity of the events and indirectly suggests the extent of the events; and the number of D100 that directly depicts the persistence of the extremely heavy precipitation. Except for the number of D100, the differences between the different categories were significant at the 90% confidence level. This suggests that the comprehensive intensity index defined as Eq. (1)

Table 2. Index definitions.

Index	Data Source	Definition
A	Gridded data	$\sum_{\text{Event rainband}} \frac{\text{Total rainfall over a grid cell}}{\text{Climatic mean of summer rainfall over the same grid cell}}$
B	Station observations	$\sum_{\text{Event rainband}} \frac{\text{Numbers of D50 for a station}}{\text{Climatic mean of D50 in summer for the same station}}$
C	Station observations	$\frac{\text{Numbers of stations with total rainfall over 300 mm}}{\text{Numbers of stations with total rainfall over 100 mm}}$

Table 3. PHR event categories by occurrence, intensity index, and PDF*.

Category	Occurrence	Range of Intensity Index	PDF
Most severe	17	< 100	0.0719
Severe	45	100–230	0.2377
Moderate	68	230–360	0.3701
Weak	56	360–500	0.2542
Weakest	11	> 500	0.0661

*Probability density function

Table 4. PHR event Categories by major attribute.

Category	Length (days)	Extent (No. of grid cells)	Areal Rainfall (10^3 mm km^2)	Maximum Total rainfall* (mm)	A	B	No. of D100
Most Severe	14	784	181526	797.6	226.07	43.41	8
Severe	9	468	85962	525.3	102.63	24.28	4
Moderate	7	305	49612	471.0	55.01	14.89	3
Weak	6	202	31818	428.3	32.00	8.45	3
Weakest	5	113	17333	307.4	15.89	5.73	1

*Based on weather station observations.

Table 5. PHR flow regime backgrounds and occurrence.

Regime	Related Features	Occurrence	Percentage
W	Shear, vortices, jet stream, trough	81	62%
E	Typhoon, tropical cyclone, ITCZ, easterly wave	27	21%
W/E	Interaction of westerly and easterly disturbances	22	17%

is suitable for describing PHR events quantitatively. Thus, to achieve the goal of this study, we will focus further analyses on the first three categories (the most severe, severe, and moderate) of the PHR events, of which there are 130.

After defining PHR events, we identified both the geographic location of each event rainband and the average large-scale circulation background of each event. Then we classified the events in several ways to reveal event features. Based on the different classifications, we investigated the characteristics of the spatial and temporal distributions of PHR events by means of synoptic, composite, and statistical analyses.

4. Results

The characteristics of PHR events varied, depending on where, when and under which circulation background the events occurred. Thus, we will describe the general characteristics of the PHR events first, followed by their spatial and temporal distributions. Finally, we will depict the characteristics of the first two categories, most severe and severe, of PHR events according to their geographical locations.

4.1 *The general characteristics of the PHR events*

To more objectively study the characteristics of these PHR events in China, we classified the 130 events into 3 types according to the circulation backgrounds of East Asia; and into 8 groups based on event rainband locations. The results of these classifications are described in the following paragraphs.

The causes of PHR events are indisputably very complicated since the causes of summer precipitation in China are very complex (Ding, 1992; Samel et al., 1999; Zhang et al., 2002; Huang and Zhou, 2003; Tang, 2004). Although the details of the specific atmospheric circulation patterns and synoptic systems responsible for PHR events are beyond the scope of this study and will be addressed later, grouping the events according to their large scale circulation backgrounds proves to be helpful. For that purpose, we reviewed daily and the event-averaged wind and geopotential height fields

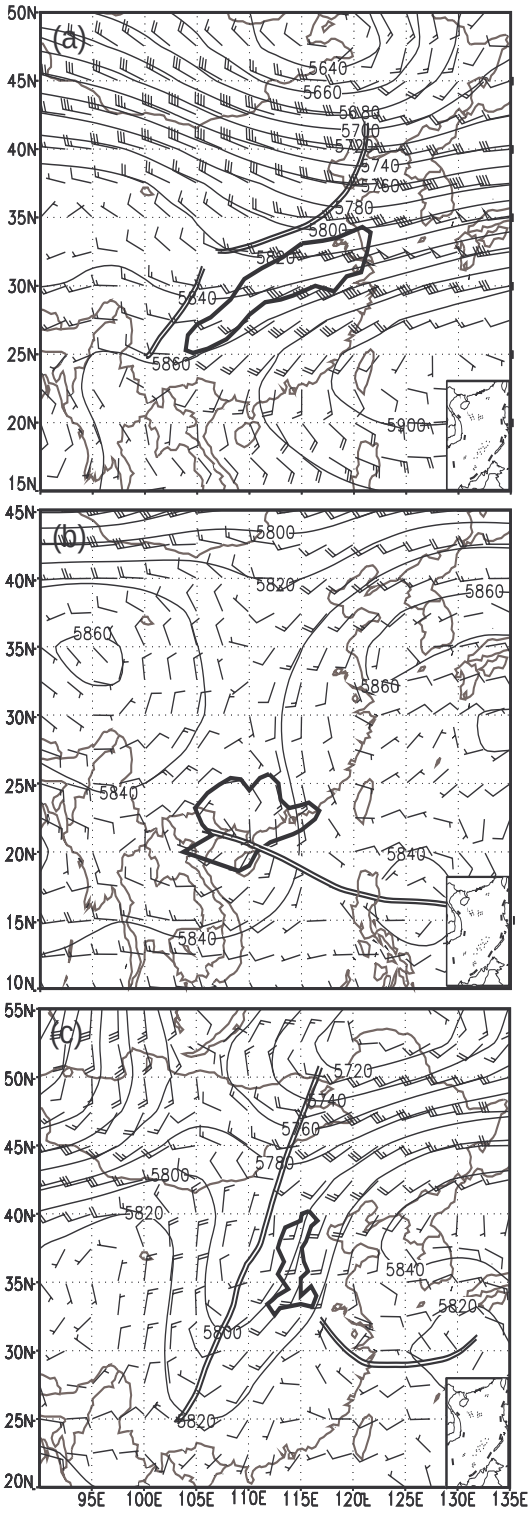

Fig. 2. Average 500-hPa geopotential height contours and wind barbs for events of (a) 29 June to 11 July 1991; (b) 14–31 July 1994 and (c) 2–10 August 1963. The areas shown by the thick solid line are the event rainband. The double solid line indicates either trough or convergent zone.

at 500 hPa for all events. According to the prevailing wind flow pattern over event rainbands, PHR events were subdivided into three types (Table 5), a westerly regime (W), an easterly regime (E) and convergence of westerly and easterly regimes (W/E). Fig. 2 shows the event-averaged wind and geopotential height fields at 500 hPa of a typical event for each type. The average circulation during 29 June–11 July 1991, typical of the W-regime (Fig. 2a), revealed that the prevailing wind flow over the event rainband was westerly in the northwest flank of a stable zonal subtropical high, along which a series of low-level disturbances, including trough, vortices, and jet-stream, continually propagated eastward and caused persistently intense precipitation. Figure 2b, the average circulation during 14–31 July 1994, showed typical features of E-regime events. The event rainband was stable under the control of the ITCZ in the southwest flank of a subtropical high over the Sea of Japan. Typhoons and tropical depressions moving northwestward were responsible for persistent heavy rainfall. The average circulation of a typical W/E-regime event that occurred during 2–10 August 1963 is depicted in Fig. 2c. The convergence of the ITCZ and westerly trough, which are located to the south and west of the West Pacific subtropical anticyclone respectively, led to the generation of an intense rainband. The interaction of westerly disturbances and tropical perturbations yielded copious quantities of rainfall.

The major circulation background associated with PHR events in China was the westerly regime. More than half (81 cases, 62%) of the 130 cases and 82% (14/17) of the most severe cases were induced by westerly disturbances. However, the easterly regime also played an important role in the occurrence of many PHR events, as did interactions between westerly and easterly flow regimes.

Research demonstrates that the characteristics of summer precipitation in China are strongly influenced by different geographical settings (Ding, 1992; Zhang and Lin, 1992; Samel et al., 1999; Yu et al., 2001; Tang, 2004). Therefore, we classified the 130 events into eight regions according to the locations of their rainbands. Regions (Fig. 3) were defined as those areas marked by high frequencies of rainbands. As shown in the figure, the eight regions characterized by event rainbands are Northeast China (NE, Fig. 3a), North China (NC, Fig. 3b), Huaihe River valley (HR, Fig. 3c), Yangtze River-Huaihe River valley (YH, Fig. 3d), Yangtze River valley (YZ, Fig. 3e), south of the Yangtze River (YS, Fig. 3f), southeast coast (ES, Fig. 3g) and Southwest China (WS, Fig. 3h). The frequencies of events under the three types of regimes are pre-

Table 6. PHR event frequencies by regions, categories, and regimes.

		Category									
		1*			1+2*			1+2+3*			
		Regime			Regime			Regime			
Region	Abbr.	W	W/E	E	W	W/E	E	W	W/E	E	Total
Northeast China	NE	0	0	0	0	2	0	0	4	0	4
North China	NC	0	1	0	0	2	0	0	4	0	4
Huaihe River Valley	HR	1	0	0	4	0	0	7	0	0	7
Yangtze River-Huaihe River Valley	YH	5	0	0	9	0	0	14	0	0	14
Yangtze River Valley	YZ	1	0	0	5	0	0	11	0	1	12
South of the Yangtze River	YS	5	1	0	17	2	1	29	2	1	32
Southeast Coastal Area	ES	2	0	0	5	4	5	14	7	12	33
Southwest China	WS	0	0	1	1	1	4	6	5	13	24
Subtotal		14	2	1	41	11	10	81	22	27	
Total		17			62			130			130

*1 refers to the most severe cases; 1+2 the most severe and severe cases, and 1+2+3 the most severe, severe and moderate cases.

Table 7 PHR event rainband orientations by region and regime.

Region	N-S		NE-SW		E-W		NW-SE		Cluster	
	W	W/E and E	W	W/E and E	W	W/E and E	W	W/E and E	W	W/E and E
NE	0	3	0	1	0	0	0	0	0	0
NC	0	4	0	0	0	0	0	0	0	0
HR	1	0	5	0	1	0	0	0	0	0
YH	0	0	11	0	3	0	0	0	0	0
YZ	0	1	5	0	6	0	0	0	0	0
YS	0	0	23	3	5	0	0	0	1	0
ES	0	0	8	10	1	1	2	0	3	8
WS	0	0	1	1	1	0	0	4	4	13
Subtotal	1	8	53	15	17	1	2	4	8	21
Total	9		68		18		6		29	

* The figures in bold indicate the dominant shape in each region.

sented in Table 6.

4.2 *Spatial distribution of PHR events*

When the occurrences of PHR events are classified by regions in China, the resulting frequencies show that these events favor some places more than others (Table 6). High frequencies favor the following regions: ES (33 events), YS (32), and WS (24). In contrast, low frequencies favor North China and Northeast China. Moreover, if only the highest two categories of PHR events are considered, the most favored regions are YS (20 events) followed by ES (14 events). However, if the percentage frequencies of the first two categories in each region are considered, the most severely vulnerable area is YH. Of 14 events that occurred in YH during the last 50 years, 9 (about 64%) were classified as either severe or most severe events. Also, the frequencies of PHR events generally decreased northward, a spatial trend that agrees well with the climatic background (Zhang and Lin, 1992). However, the severity of the events did not vary in the same way. The percentage of severe or most severe events in NC (2 cases, 50%) is much higher than that in WS (6 cases, 25%).

The frequencies of PHR events under different circulation regimes varied in different regions (Table 6). In general, westerly disturbances were the major causes of PHR events (81/130, 62%), especially in the regions of YH (100%), HR (100%), YZ (92%) and YS (90%). However, this does not apply to other regions. PHR events induced directly or indirectly by tropical disturbances were abundant in WS (18 cases, 75%) and ES (19 cases, 58%). Moreover, tropical disturbances

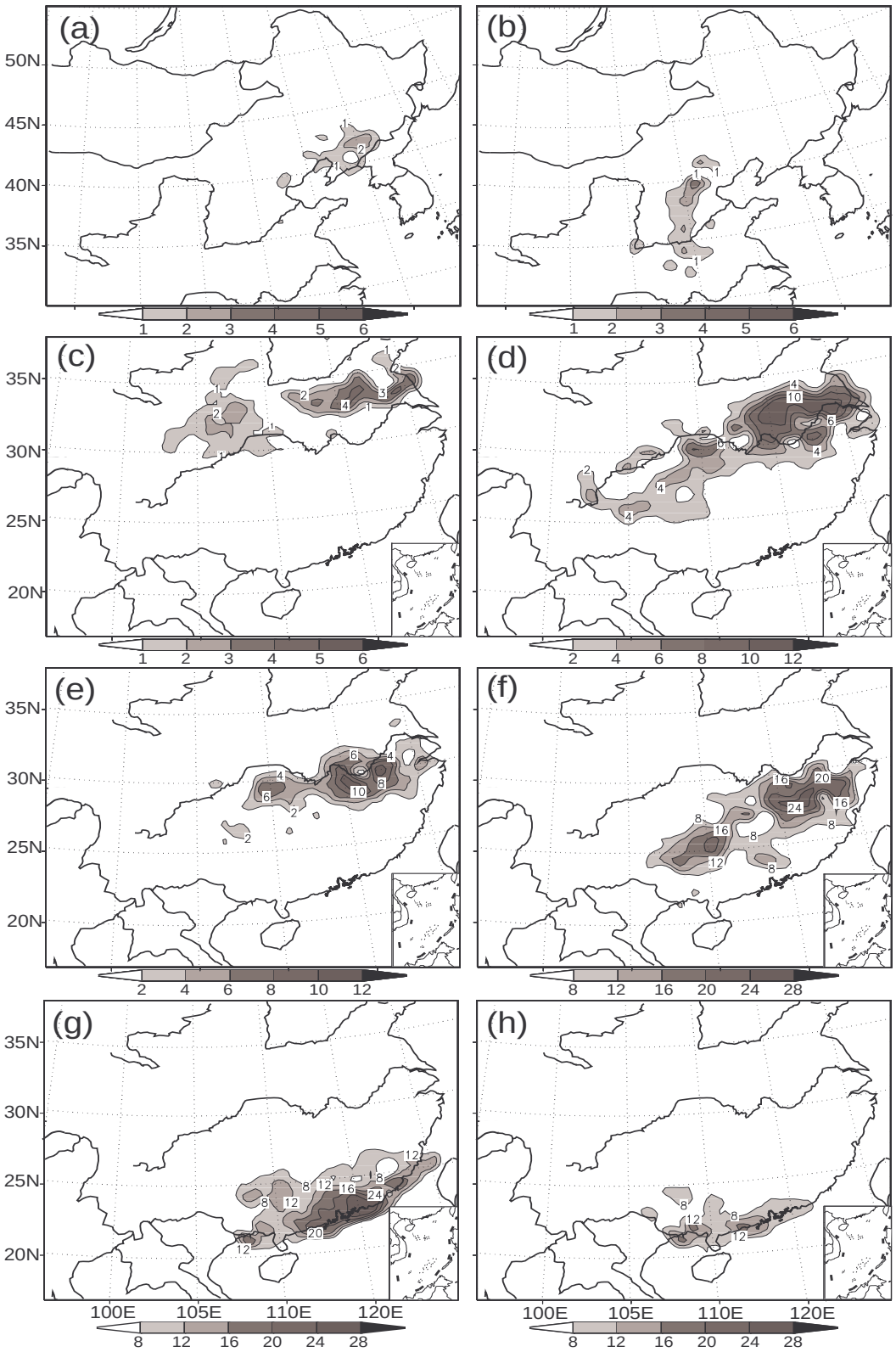

Fig. 3. Total numbers of PHR events occurring during the summer season of 1951–2004 in the different groups of (a) Northeast China (NE); (b) North China (NC); (c) Huaihe River valley (HR); (d) Yangtze River-Huai River valley (YH); (e) Yangtze River valley (YZ); (f) South of the Yangtze River (YS); (g) Southeastern coastal area (ES); (h) Southwest China (WS).

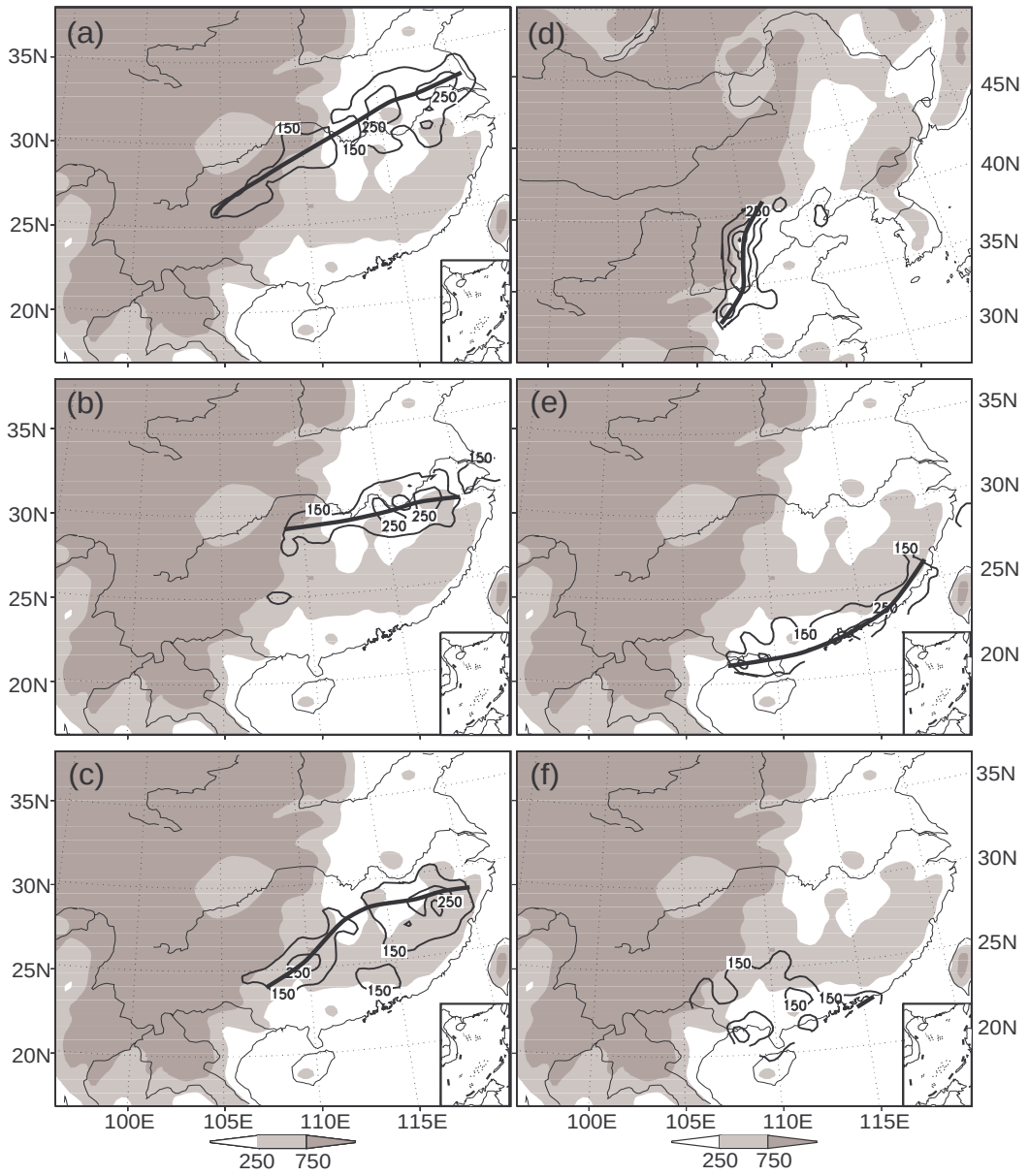

Fig. 4. The mean event accumulated precipitation for two circulation backgrounds of W-regime (a–c) and E-and W/E-regime (d–f), in different regions of (a) the Yangtze River-Huaihe River valley (YH); (b) the Yangtze River valley (YZ); (c) south of the Yangtze River (YS); (d) North China (NC); (e) the southeastern coastal area (ES); (f) southwest China (WS). The interval of isohyets is 150 mm. The two shaded areas indicate terrain heights over 250 m and 750 m respectively. The thick line denotes the axis of event rainband.

even played a major role in generating PHR events occurring in Northern China. All events identified in this region, including NC and NE, were induced by the interaction of middle latitude and tropical disturbances. An event occurring in the North China Plain during 2–10 August 1963 provides a good example. The facts revealed here agree well with other work (Li et al., 2004).

Each PHR possessed a coherent event rainband. Rainband orientation is defined by the orientation of the rainband axis. On the whole, the shapes of event rainbands resembled either belts or clusters. Belt shapes mainly characterized events with westerly regimes. Cluster rainbands often accompanied events resulting either directly or indirectly from easterly disturbances. Clusters appeared in South China only. Regional rainband characteristics are presented in Table 7. Five orientations were recognized: north-south

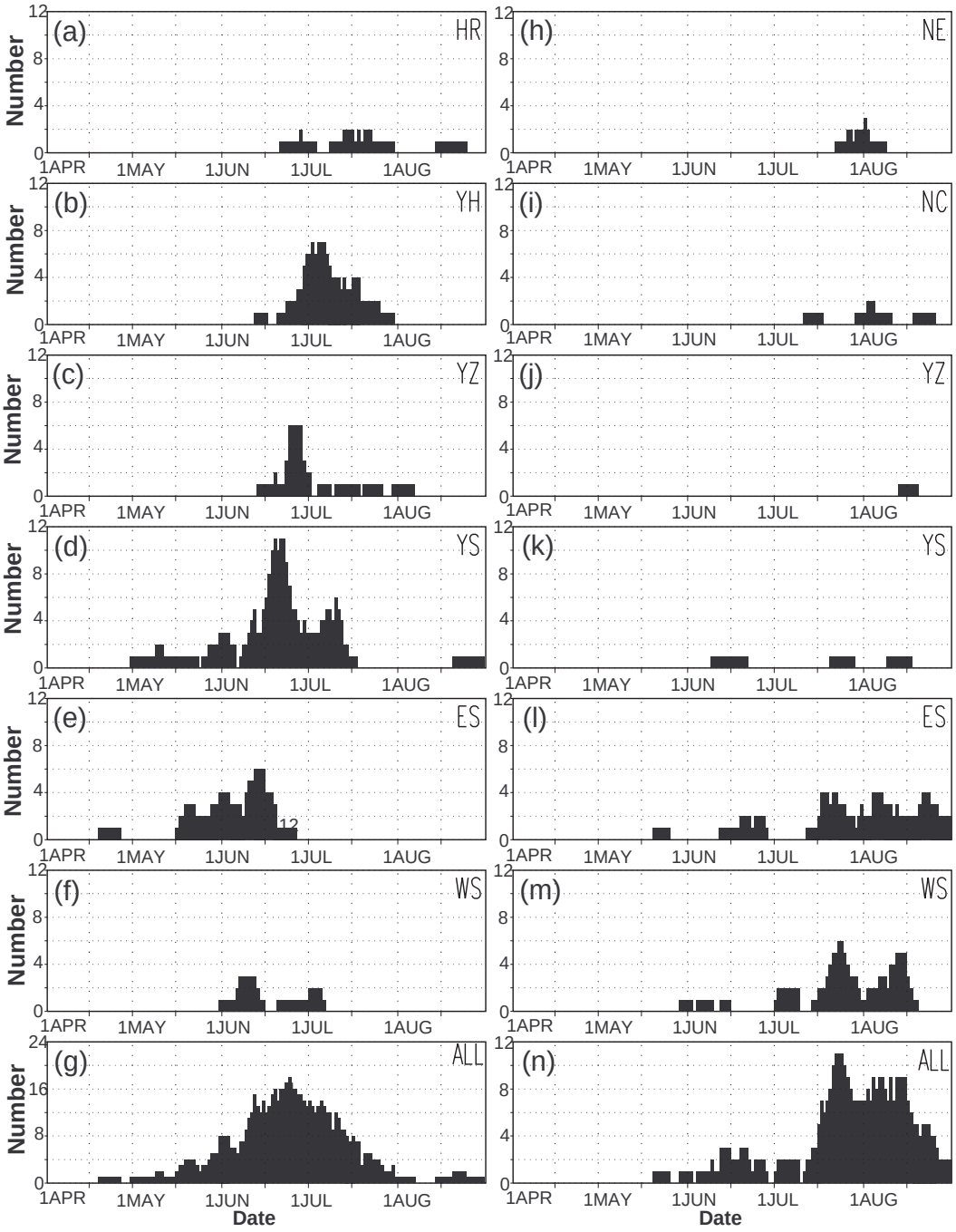

Fig. 5. Total numbers of the events occurring during each day in the summer of 1951–2004 for two circulation backgrounds of W-regime (a–g) and E- and W/E-regime (h–n) in the different regions of (a) HR; (b) YH; (c) YZ; (d) YS; (e) ES; (f) WS; (g) all groups; and (h) NE; (i) NC; (j) YZ; (k) YS; (l) ES; (m) WS; (n) all groups.

(N-S, 9 events, 7%), northeast-southwest (NE-SW, 68 events, 52%), east-west (E-W, 18 events, 14%), northwest-southeast (NW-SE, 6 events, 5%) and cluster (29 events, 22%). Clearly the more common orientations for events with a W regime were NE-SW (53/81, 66%) and E-W (17/81, 21%). Similarly, the most common orientation for events induced by easterly disturbances was cluster (21/49, 43%). In addition, differences in the orientations of event rainbands among the different groups were distinctive. The fig-

ures in bold in Table 7 denote the rainband shapes dominant in each region. N-S orientations ruled in NE and NC, whereas clusters and NW-SE orientations reigned in southern China including ES and WS. NE-SW and E-W orientations prevailed over an extensive area including YS, YH, YZ, and HR. Fig. 4 shows the composite shapes and orientations of events by averaging a set of the event rainbands with the same regime from different regions. The orientation of event rainbands depends considerably on local geographical settings and topographical features.

As stated earlier, the most typical shape of event rainbands is like a belt with a NE-SW orientation (Figs. 4a–c, e) in all regions except in northern China and WS. When a belt appeared under the westerly regime, it was actually part of the main rainband of the East Asian summer monsoon, which was located on the northwestern flank of the subtropical high and which shifted northwards or southwards during the warm season (Ding, 1992; Samel et al., 1999). A total of 13 out of 14 (93%) of the most severe events resulted from westerly disturbances that possessed this type of event rainband. As for northern China, including both NC and NE, the event rainband was also belt-shaped, but its axis tended to be oriented S-N (Fig. 4d). This orientation stems from meridional circulations and local orographic conditions as shown in Fig. 4d (shaded area). There were 9 events identified with this type of rainband. Of these 9, 8 were induced either indirectly (7 cases) or directly (1 case) by tropical disturbances. In contrast with other regions, zones of maximum precipitation usually appeared as clusters or as belts oriented NW-SE in the WS (Fig. 4f). These unique rainband shapes are associated with tropical disturbances along the stable ITCZ oriented as NW-SE. Besides, local terrain effects, which block the movement of tropical disturbances, also contribute significantly to the orientation of the event rainband, since the Tibetan Plateau bounds this area on the west.

4.3 *Temporal distribution of PHR events*

The temporal distribution of PHR events has been investigated on monthly, interannual and interdecadal scales.

4.3.1 *Monthly distribution*

The distribution by months of the 130 PHR events shows that these events were most abundant in June, followed by July (Table 8). About 71% of the 130 events occurred in these two months. Figure 5 presents the distributions of the daily frequency of PHR events in different regions with different circulation backgrounds. It shows that PHR active periods in different geographical regions depended on regional climates and were closely related to the onset and retreat of the rainy season. Onset dates of PHR events were delayed northward, an observation that agrees well with the meridional shift of the summer monsoon (Lau, 1992; Ding, 1992; Samel et al., 1999). The data show that PHR events took place from mid April to late August. The first event, associated with westerly disturbances, started on 19 April 1961, and the last occurred on 24 August 1960. Both events took place in the southeast region but had different regimes. Inspection of the precipitation data reveals that the PHR active period in southern China is longer than in the northern part. Therefore, the higher frequencies of PHR observed in southern China probably reflect this disparity.

It should be noted that the active period and onset time of events with different large-scale circulation regimes also differed. In general, W-regime events prevailed in June and July, and E- (or W/E) regime events prevailed in July and August but never in April. The active period of W-regime events extended from late April to August, with a frequency peak in June and early July. Conversely, the active period of E- (or W/E) regime events was from late May to August with the maximum frequency occurring in late July and August. Besides, the active period and the onset time of events with different circulation regimes varied in different regions (Fig. 5). As mentioned above, the shift of the active period was closely associated with the meridional shift of the summer monsoon. The highest frequency of W-regime events, for example, appeared from late May to early June in ES, from the mid June to early July in YS and YZ, and in July in YH and

Table 8 PHR event categories by monthly occurrence.

Category	Occurrence					
	April	May	June	July	August	Total
Most severe	0	2	11	2	2	17
Severe	2	2	16	18	7	45
Moderate	0	10	22	23	13	68
Total	4	14	49	43	22	130

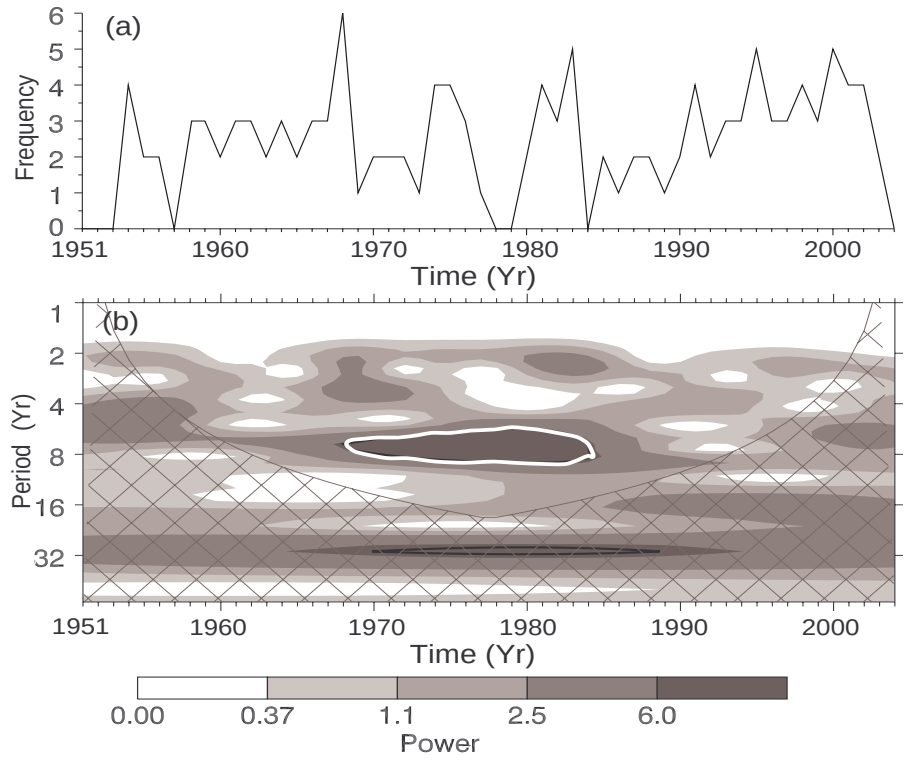

Fig. 6. (a) The annual frequency of PHR events. (b) The wavelet power spectrum via the Morlet wavelet. The contour levels are chosen so that 75%, 50%, 25%, and 5% of the wavelet power are above each level, respectively. The cross-hatched region is the cone of influence, where zero padding has reduced the variance. The black contour is the 5% significance level, using a white-noise background spectrum.

HR. In contrast, events generated either directly or indirectly by tropical disturbances often clustered in the late July and August in ES and WS, and in August in NC.

4.3.2 *Yearly distribution*

Owing to the complex interannual variability of precipitation in China (Samel et al., 1999; Yang and Lau, 2004), the annual frequency of PHR events fluctuates from year to year with the maximum amplitude of six. There are four years, 1968, 1983, 1995 and 2000, with more than 5 cases defined. On the contrary, there are seven years, 1951–1953, 1957, 1978–1979 and 1984, without any events defined. We note that the lack of early 1950s cases might be partly due to the sparse rainfall observations. Figure 6a shows the annual frequency of PHR events during the study period.

It can be seen in Fig. 6a that two periods are worth mentioning. The first period extends from 1984 to 1990. A low incidence of events is also revealed by Fig. 7, which shows the annual frequencies of events having different regimes in different regions. This low frequency period mainly reflects low frequencies of W-related events in the HR, YZ, ES, and WS regions (Figs. 7a, c, e and f). During this time, none took place in these regions. Besides, the frequencies for E-regime events in YS and WS (Figs. 7k and m) were low. The second period, from 1993 to 2002, retained a high annual frequency. Both W- and E-regime events occurred more frequently during this period, and especially significant were W-regime events in YS, YZ and HR (Figs. 7d, c, and a) and E-regime events in WS (Fig. 7f).

4.3.3 *Decadal distribution*

Figure 6 (b) shows the wavelet power spectrum via the Morlet wavelet for the annual PHR frequency time series. The wavelet power spectrum is defined as the absolute value squared of the wavelet transform and gives a measure of the time series variance at each scale (period) and at each time (Torrence and Compo, 1998). It can be seen that the power is broadly distributed, with peaks in the 6–10 yr band, although there is appreciable power at longer periods. The variance changes on the decadal scale in the frequency of PHR events are statistically significant. The 5% signi-

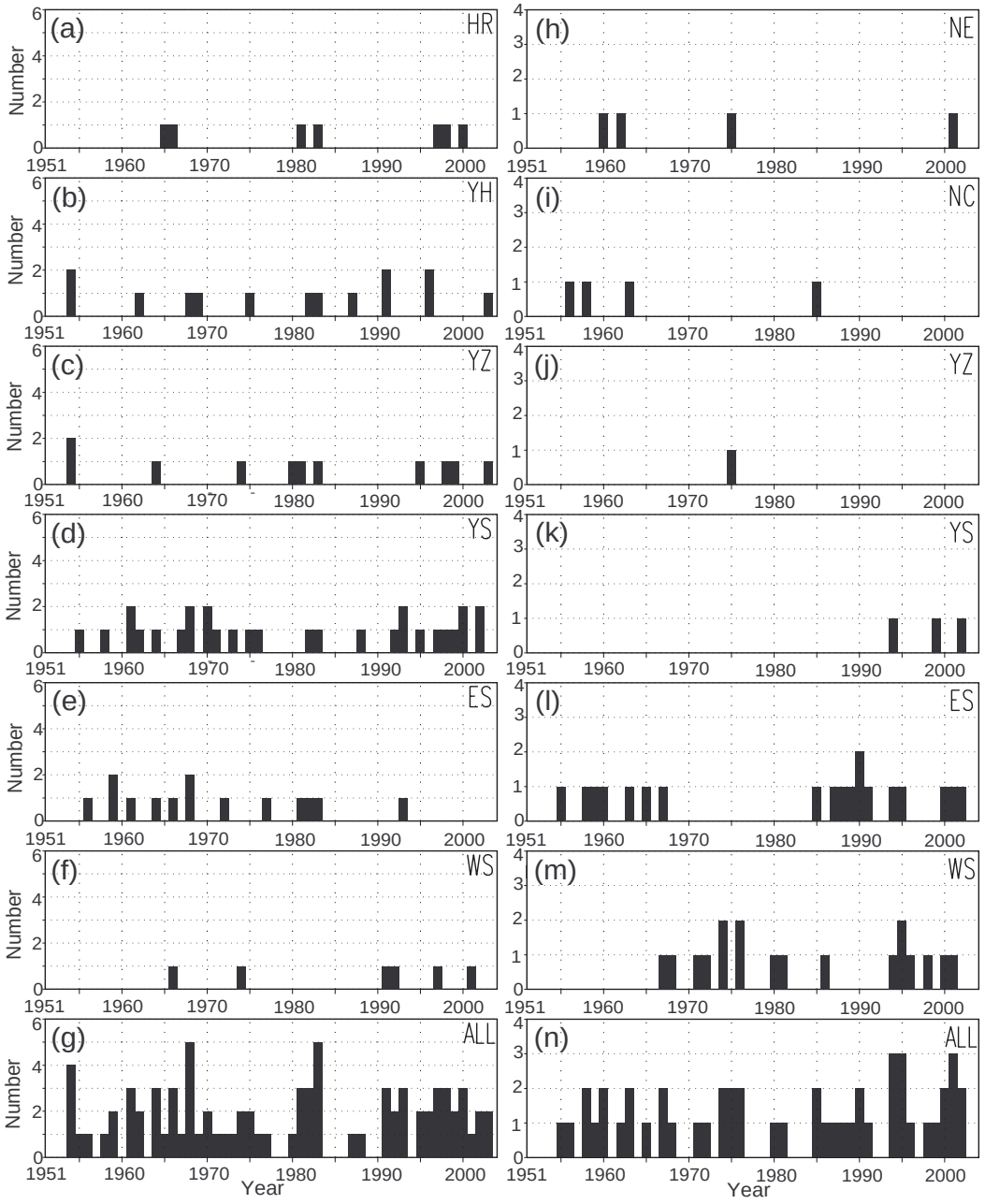

Fig. 7. Total numbers of the events occurring during the summer of each year from 1951 to 2004 for two circulation backgrounds of W-regime (a–g) and E- and W/E-regime (h–n) in the different regions of (a) HR; (b) YH; (c) YZ; (d) YS; (e) ES; (f) WS; (g) all groups; and (h) NE; (i) NC; (j) YZ; (k) YS; (l) ES; (m) WS; (n) all groups.

ficance regions (enclosed by the white contour in Fig. 6b) indicate that 1969–1984 is a time of higher frequency variance, and 1954–1968 and 1985–2003 are periods of lower frequency variance. During 1969–1984, the mean annual frequency is 2.1, which is lower than 2.7 for the period of 1954–1968 and 2.9 for 1985–2003. For different regions, the frequency distributions on the decadal scale are not same (Fig. 7), which manifests the complex space and time structures of the precipitation over China (Yang and Lau, 2004). It is the complex spatial and temporal structures that make more evident decadal variation in the frequency in different regions than in the whole country. For example, opposite trends are presented for the changes in frequencies of the E-regime events on the decadal scale in ES and WS respectively (Figs. 7l, m).

Table 9 Regional mean attributes of severe and most severe PHR events.

Region	HR	YH	YZ	YS	ES	NC	ES	WS
Onset Time	Late June – Mid July	Late June	Mid June – Mid July	Mid June	Late May – Early June	Mid July – Early August	Mid July – Late August	Mid June – Early August
Mean length (days)	9.3	14.7	8.7	15	14.3	7.7	12.7	12.3
Background	W	W	W	W	W	W/E	E	E
Mean extent (km^2)[a]	364203	761103	415197	897903	712503	245997	519597	563400
Mean maximum total rainfall (mm)	364.3	778.6	640.7	842.6	877.3	517.5	622.5	829.4
Mean areal rainfall (10^3 mm km^2)	54489	190638	101869	261550	174120	42684	107750	137782
Mean A[b] (%)	63.87	94.42	51.57	63.41	53.01	105.23	46.24	52.46
Mean B[b] (%)	172.95	188.46	108.98	157.55	90.28	251.41	87.95	87.74

[a]Extent is the number of grid cells in an event rainband multiplied by the unit grid cell area (900 km^2).
[b]The means of both A and B are derived from the three highest values recorded for each event.

4.4 *Severe and most severe events*

As stated earlier, 62 of 130 PHR events observed during the study period were classified as being either severe or most severe. Such events have been a major cause of flood disasters (Zhang et al., 2002; Xiong et al., 2003; Guo et al., 2004). Thus, we should pay special attention to them. Based on frequency analysis (Table 6), we know that these events have occurred, although not uniformly, in all regions of the study area. However, event behaviors differed according to geographical region, as well as to their large-scale circulation background. In order to emphasize this point, we used the three most severe events controlled by different regimes for each region to calculate average event attributes (Table 9). The NE region was omitted because no most severe event occurred during the study period. It is apparent that the most severe PHR events occurring in different regions with different regimes possessed their own distinctive attributes besides their common characteristics.

The PHR events recorded in northern China, including North China and Northeast China, have, on average, the shortest durations (less than 10 days) and the smallest spatial extents, but the strongest relative intensities. Their severity is borne out by the values presented in Table 9 (column 7). The values show that, on average, almost twice the mean summer total rainfall or about two and half times that of the mean heavy rain day could fall somewhere within an event's rainband. Such extreme events certainly have caused calamities with huge losses of property and even human life. The PHR events occurring in northern China usually resulted from the convergence of middle latitude systems and tropical disturbances. No severe events have been identified in this area since the 1970s because its rainfall characteristics have significantly changed (Gong et al., 2004; Huang et al., 1999; Easterling et al., 2000; Zhai et al., 1999).

The PHR events prevailing over the Yangtze River and Huaihe River valleys have received much attention because of the Mei-Yu season. The PHR event contributions to Mei-Yu rainfall are crucial because these storms generate so many major rainy spells. These PHR events usually have long durations in YH compared to those occurring in surrounding regions. Significantly, event rains are very intense. Both the mean A and B indexes for summer are only slightly lower than the cases appearing in the north (Table 9). The total areal rainfall ranks second among all groups. The event rainband, located on the northwest flank of the subtropical high with its axis at 23°–25°N, has a perfect belt shape with a NE-SW orientation. Except for the subtropical high, the major synoptic systems directly responsible for the persistent heavy rainfall in-

clude a series of low-level disturbances, including shear lines, jets, troughs, and vortices along the Mei-Yu front (Zhang et al., 2002). The event rainband shifts position with the movement of the subtropical high, since its location depends greatly on the axis of the subtropical high. When the axis is between 26°–28°N, the PHR event rainband shifts northward over the Huaihe River valley and forms the HR event rainband; and when it is at 21°–24°N, the rainband shifts southward along the Yangtze River valley and forms the YZ event rainband. However, under both conditions, the PHR events are not as severe as those occurring over YH (Table 9, columns 2–4).

The most severe PHR events occurring in YS took place in mid June. They normally had the largest extent and heaviest total areal rainfall (Table 9, column 5), but their contributions to the region's mean summer rainfall total were relatively less than those in NC and YH because of the YS region's heavier mean summer rainfall. Although the axis of the event rainband is oriented northeast-southwest, the location of the event rainband, which is closely related to the synoptic situation, is less stable than its counterparts in YH and YZ.

The southeastern coast was the only region where the numbers of severe and most severe events under the three different regimes approached equality (Table 6). The active period of the severe and most severe PHR events included May, June, July and August (Table 9, column 6 and 8). Compared to the W-regime events that occur in YS and YH, the W-regime events in ES were relatively weak, although they possessed the highest mean maximum total rainfall among all W-regime cases (Table 9, column 6). The PHR event rainband is typically oriented northeast-southwest paralleling the general coastline. In contrast, the region's E-regime events were weaker than its W-regime events (Table 9, column 8). Indeed, E-regime events were even weaker than comparable events occurring in WS.

Although a PHR event in WS set the study period record for maximum rainfall total (1313.5 mm) during 14–31 July 1994, it was less intense than the W/E-regime events that occurred in the northern part of China and the W-regime events that took place in YH and YS. This lower intensity was a consequence of the more abundant summer rainfall in this area. According to Table 6, the percentage (25%) of the severe and most severe events in this region was the lowest for the period of study.

5. Conclusions

Based on gridded daily rainfall and station daily rainfall for China for the period of 1951–2004, a semi-quantitative approach was followed to identify PHR events. The characteristics of PHR events were then investigated. The study focus was directed mainly on severe and most severe events that took place over more than 50 years. The main conclusions of the study are as follows.

(1) PHR events occurred mainly in eight geographical regions: North China, Northeast China, the Huaihe River valley, the Yangtze River-Huaihe River valley, the Yangtze River valley, south of the Yangtze River, the southeast coastal area, and Southwest China. PHR event frequency was greatest south of the Yangtze River and on the southeast coast. The highest percentages of severe and most severe storms struck the Yangtze River and Huaihe River Valleys, making this the most vulnerable region for the study period.

(2) Based on the large-scale circulation background over an event rainband, PHR events can be classified into three regimes: westerly, easterly, and interacting westerly/easterly. The regions typified by each regime are central China (including the Yangtze River-Huaihe River valley, along the Yangtze River and areas nearby) for W-regimes; southern China (including southeast coastal and southwest areas) for E-regime events, and northern China (including North China and Northeast China) for W/E regimes. Event rainbands exhibited two general forms: clustered and belted with either a N-S, NE-SW, E-W, or NW-SE orientation. The most common form was belt-shaped oriented either NE-SW or E-W. This shape was usually associated with westerly regime events occurring within an extensive area south of the Yellow River. The cluster-type rainband mainly appeared in southern China in those cases with the easterly regime. The belt-shaped rainband with a N-S orientation is also common in the cases with the easterly/westerly regime background in the northern part of China.

(3) Westerly regime events generally took place during June and the first half of July. Easterly regime and easterly/westerly regime events were most typical during the last half of July and August.

(4) The characteristics of PHR events with different regimes differed. Normally, PHR events with the westerly regimes exhibited longer durations, were wider, and occupied larger areas than easterly or easterly/westerly regimes. The shapes of event rainbands associated with events having easterly regimes were more complicated than those with westerly regimes.

(5) Interannual and interdecadal variations in the frequency of PHR events were characteristic in China during the study period.

It is hoped that this study of PHR events in China provides a basis for the discovery and understanding

of processes that generate these events under different synoptic conditions.

Acknowledgments. NCEP Reanalysis data used in this study were provided by the NOAA-CIRES Climate Diagnostics Center, Boulder, Colorado, USA, from their web site at http://www.cdc.noaa.gov. The authors wish to thank Professor John Donahue for his help in improving the English of the manuscript. This work was supported by the National Natural Science Foundation of China under Grant No. 40575015.

REFERENCES

Ding Yihui, 1992: Summer monsoon rainfalls in China. *J. Meteor. Soc. Japan*, **70**, 373–396.

Easterling, D. R., G. A. Meehl, C. Parmesan, S. A. Changnon, T. R. Karl, and L. O. Mearns, 2000: Climate extremes: Observations, modeling, and impacts. *Science*, **289**, 2068–2074.

Gong, D-Yi, P-J. Shi, and J-G. Wang, 2004: Daily precipitation changes in the semi-arid region over northern China. *Journal of Arid Environments*, **59**, 771–784.

Guo Yufu, Wang Jia, and Zhao Yan, 2004: Numerical simulation of the 1999 Yangtze River valley heavy rainfall including sensitivity experiments with different SSTA. *Adv. Atmos. Sci.*, **21**, 23–33.

Huang Ronghui, and Zhou Liantong, 2003: The progresses of recent studies on the variabilities of the East Asian monsoon and their causes. *Adv. Atmos. Sci.*, **20**, 55–69.

Huang Ronghui, Xu Yuhong, and Zhou Liantong, 1999: The interdecadal variation of summer precipitations in China and the drought trend in North China. *Plateau Meteorology*, **18**, 465–476. (in Chinese)

Kalnay, E., and Co-authors, 1996: The NCEP/NCAR 40-year reanalysis project. *Bull. Amer. Meteor. Soc.*, **77**, 437–471.

Karl, T. R., and K. E. Trenberth, 2003: Modern global climate change. *Science*, **302**, 1719–1723.

Lau, K. M., 1992: East Asian summer monsoon rainfall variability and climate teleconnection. *J. Meteor. Soc. Japan*, **70**, 211–242.

Li Yuefeng, Luo Yong, and Ding Yihui, 2004: The relationships between the global satellite-observed outgoing longwave radiation and the rainfall over China in summer and winter. *Advances in Space Research*, **33**, 1089–1097.

Liu Shuyuan, Zheng Yongguang, Wang Hongqing, and Wu Qingli, 2002: Analyses of heavy rain in Huaihe River Basin during 28 June–2 July 1998. *Acta Meteorologica Sinica*, **60**, 774–779. (in Chinese)

Samel, A. N., W.-C. Wang, and X. Z. Liang, 1999: The monsoon rainband over China and relationships with the Eurasian circulation. *J. Climate*, **12**, 115–131.

Tang Yanbing, 2004: Connections between the surface sensible heat net flux and regional summer precipitation over China. *Adv. Atmos. Sci.*, **21**, 897–908.

Torrence, C., and G. P. Compo, 1998: A practical guide to wavelet analysis. *Bull. Amer. Meteor. Soc.*, **79**, 61–78.

Trenberth, K. E., A. Dai, R. M. Rasmussen, and D. B. Parsons, 2003: The charging characters of precipitation. *Bull. Amer. Meteor. Soc.*, **84**, 1205–1217.

Trialo, M. F., 2003: *Elementary Statistics*. USA: Addison Wesley, 864pp.

Xiong Zhe, Wang Shuyu, Zeng Zhaomei, and Fu Congbin, 2003: Analysis of simulated heavy rain over the Yangtze River valley during 11–30 June 1998 using RIEMS. *Adv. Atmos. Sci.*, **20**, 815–824.

Yang Fanglin, and K. M. Lau, 2004: Trend and variability of China precipitation in spring and summer: Linkage to sea-surface temperatures. *International Journal of Climatology*, **24**, 1625–1644.

Yu Rucong, Zhang Minghua, Yu Yongqiang, and Liu Yimin, 2001: Summer monsoon rainfalls over mid-eastern China lagged correlated with global SSTs. *Adv. Atmos. Sci.*, **18**, 179–196.

Zhai Panmao, Ren Fumin, and Zhang Qiang, 1999: Detection of trend in China's precipitation extremes. *Acta Meteorologica Sinica*, **57**, 208–216. (in Chinese)

Zhang Jiachen, and Lin Zhiguang, 1992: *Climate of China*. Shanghai Scientific and Technical Press, 603pp.

Zhang Shunli, Tao Shiyan, Zhang Qingyun, and Wei Jie, 2002: Multi-scale circulation conditions of heavy rainfall in the middle and lower ranges of the Yangtze River basin. *Chinese Science Bulletin*, **47**, 467–473. (in Chinese)